



Microstructures and magnetic properties of Co-substituted Ce–Fe–B amorphous alloys



Dan Liu^a, Tongyun Zhao^b, Baogen Shen^{b,*}, Baohe Li^{a,**}, Ming Zhang^c, Shulan Zuo^b, Jun Liu^b, Sida Jiang^d, Fengxia Hu^b, Jirong Sun^b

^a Department of Physics, School of Sciences, Beijing Technology and Business University, Beijing, 100048, PR China

^b State Key Laboratory of Magnetism, Institute of Physics, Chinese Academy of Sciences, Beijing, 100190, PR China

^c School of Physics, Inner Mongolia University of Science and Technology, Baotou, 014010, PR China

^d School of Materials Science and Engineering, Harbin Institute of Technology, Harbin, 150001, PR China

ARTICLE INFO

Article history:

Received 18 August 2019

Received in revised form

12 November 2019

Accepted 18 November 2019

Available online 19 November 2019

Keywords:

Ce–Fe–B magnets

Amorphous ribbons

Co-doped

Micromagnetic simulation

ABSTRACT

Compare with Ce–Fe–B crystalline magnets, the amorphous alloy exhibit interesting properties due to their domains, low anisotropy energy, and microstructure contribution. In order to investigate magnetic properties and microstructures of the amorphous Ce–Fe–B system with Co substituting for Fe, the ribbons with a nominal composition of $\text{Ce}_{13.5}(\text{Fe}_{79.5-x}\text{Co}_x)\text{B}_7$ ($x = 0, 3, 6, 9, 12$) were prepared using vacuum melt spinner at a wheel speed of 50 m/s. The XRD and the corresponding SAED Pattern indicate the uniform amorphous microstructure is well maintained in each sample. These ribbons are magnetically soft and undergo a second order phase transition from ferromagnetic to paramagnetic state. With the increasing Co content, the Curie temperature almost linearly increases with temperature during 270 K and 410 K. Results from Lorentz Transmission Electron Microscopy (L-TEM) and micromagnetic simulation prove that the vortex domains can form spontaneously and stability in Ce–Fe–B amorphous materials no matter doping Co or not. The nontrivial topological domain structures found in experiments and numerical calculations have potential applications in the field of information storage, which is helpful to develop new applications of high abundance rare earth elements in functional materials.

© 2019 Elsevier B.V. All rights reserved.

1. Introduction

Amorphous magnetic materials usually have very unique mechanical, chemical and physical properties due to their disordered structure, which is an important research object in physics and material science [1,2]. In addition to being widely used in industry, agriculture, medical treatment and daily life, amorphous materials also play an important role in supporting high-tech fields such as electronic information, energy, national defense and aerospace. In the information industry, the amorphous glass composite fiber is the key material of modern communication. The materials with vortex magnetic domains presenting potential applications for high-density information data storage and spintronic devices because of their topological properties and efficient current-driven behavior. Meanwhile, the heavy rare-earth amorphous film can be

used as magneto-optical recording materials due to the relatively large Kerr rotation angle [1,3]. In energy terms, the development and utilization of amorphous materials are of great significance to promote energy conservation and environmental protection. For example, Fe-based amorphous materials are used in the manufacture of the transformer because of their high magnetic induction intensity and low eddy current loss [4–6]. In the field of national defense, glass fiber reinforced amorphous composites are widely used in the manufacture of military aircraft and missiles [7]. In the space field, due to the high specific strength, high elastic limit and other characteristics of amorphous alloy, it is expected to be used in space vehicles, such as satellite solar battery and disc compression bar of the space probe extension mechanism [8].

As the first element with 4f electrons in the lanthanide, the phase diagram of the cerium (Ce) alloy is relatively complicated. It can be paramagnetic, antiferromagnetic or superconducting under different pressure and temperature conditions. Like other amorphous materials, Ce-based amorphous alloys have no magneto-crystalline anisotropy or the magnetocrystalline anisotropy caused

* Corresponding author.

** Corresponding author.

E-mail addresses: shenbaogen@yeah.net (B. Shen), lbhe@btbu.edu.cn (B. Li).

by structural order is very weak because of the disordered arrangement of atoms. There are also no substances, such as grain boundary phase, grain boundary and dislocation inside the material that prevents the domain walls from moving. As a result, the material has low coercivity, high permeability and excellent soft magnetic properties [9,10]. In addition, the minimum glass transition temperature of Ce-based amorphous material can reach 68 °C, indicating that its amorphous state can maintain strong stability near room temperature. The thin strip or thin film of Ce-based amorphous alloys have the potential of miniaturization, high magnetic recording density and high output characteristics in information storage [11,12]. Z.B. Li et al. [13] found that the $\text{Ce}_{13-x}\text{Fe}_{81+x}\text{B}_6$ ($x = 0, 0.5, 1, 1.5, 2$) amorphous magnets had strong soft magnetic characteristics at low temperature. For the magnetic field changes of 0–2 T and 0–5 T, the refrigeration capacities are in the ranges of 116–150 J/kg and 319–420 J/kg respectively, which can be comparable with conventional magnetic materials for room-temperature refrigeration. From the perspective of balanced utilization of resources, Ce based amorphous material is a kind of materials with important theoretical and practical value due to the low cost and simple preparation process. The study of Ce–Fe–B amorphous alloy can not only supplement the fundamental understanding of Ce–Fe–B materials, but also greatly expand the application of high abundance rare earth elements in functional materials.

In the experiment, amorphous $\text{Ce}_{13.5}(\text{Fe}_{79.5-x}\text{Co}_x)\text{B}_7$ ($x = 0, 3, 6, 9, 12$) ribbons were prepared by melt rapid quenching method. And the intrinsic properties and magnetic domains of the $\text{Ce}_{13.5}(\text{Fe}_{79.5-x}\text{Co}_x)\text{B}_7$ amorphous system were systematically investigated. At the same time, the finite difference method of micro-magnetism is used to study the relationship between the magnetocrystalline anisotropy and equilibrium magnetization distribution of Ce–Fe–B alloys.

2. Experiment

The Polycrystalline $\text{Ce}_{13.5}(\text{Fe}_{79.5-x}\text{Co}_x)\text{B}_7$ ingots with $x = 0, 3, 6, 9$ and 12 were synthesized from the mixture of high-purity Ce, Fe, Co, and Fe–B alloys by arc melting under argon atmosphere. Each ingot was remelted five times to promote the composition homogeneity and then crushed into small pieces and inserted into a quartz tube with an orifice diameter of 0.5 mm. The ribbons about 1 mm wide and 10 μm thick were obtained directly by induction melting the pieces and then ejecting the melt through the orifice onto a copper roll rotating at the velocity of 50 m/s. The amorphous state of melt-spun ribbons was confirmed by X-ray diffraction (XRD) using $\text{Cu K}\alpha$ radiation. The magnetic measurements were performed using the Superconducting Quantum Interference Device Vibrating Sample Magnetometer (SQUID VSM). In addition, the microstructure and magnetic domain structure were observed using Lorentz transmission electron microscopy (L-TEM). The L-TEM samples were cut from ribbons and thinned via focused ion-beam (FIB) method and conventional ion milling method, respectively. The L-TEM image was taken at room temperature with a scale bar of 1 μm .

3. Results and discussion

The XRD patterns of $\text{Ce}_{13.5}(\text{Fe}_{79.5-x}\text{Co}_x)\text{B}_7$ ($x = 0, 3, 6, 9, 12$) melt-spun ribbons at wheel speed of 50 m/s were characterized in Fig. 1. The samples show no obvious indication of diffraction peaks, but exhibit a broad maximum at around 43°. Such bumps are characteristic of amorphous structures which suggest that the melt-spun ribbons are essentially in the amorphous state. In the process of experimental preparation, it is found that the substitution of Fe with Co will increase the difficulty of forming the amorphous state

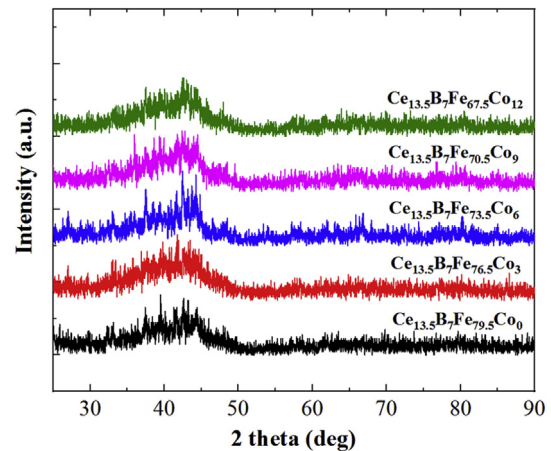


Fig. 1. The XRD patterns of $\text{Ce}_{13.5}(\text{Fe}_{79.5-x}\text{Co}_x)\text{B}_7$ ($x = 0, 3, 6, 9, 12$) ribbons for different Co content prepared by melt spinning method using a vacuum melt spinner at wheel speed of 50 m/s.

of Ce–Fe–B alloy. The replacement of Co atom leads to the short-range ordered arrangement of atoms, which improves the magnetic order and makes it more difficult to form amorphous state [14].

There is neither volume nor structural change accompanying the magnetic phase transition in amorphous magnets since its atomic arrangement is in long-range disorder. The Curie temperature (T_c) of amorphous materials reflects the short range order in the structure, which is an important index of practical application. The working temperature of amorphous magnetic materials generally cannot exceed the Curie temperature. Fig. 2 shows the temperature dependence of magnetization for all as-spun amorphous ribbons measured in an applied external field of 500 Oe. The magnetizing curves declined sharply with the increase of temperature, indicating the occurrence of a magnetic phase transition. At room temperature, the substitution of Fe atoms with Co atoms makes the compound change from paramagnetic to ferromagnetic. The inset shows the Curie temperature which determined by the maximum of dM/dT [15]. The Curie temperature of $\text{Ce}_{13.5}\text{Fe}_{79.5}\text{B}_7$ spun ribbons, corresponding to the ferro-to-

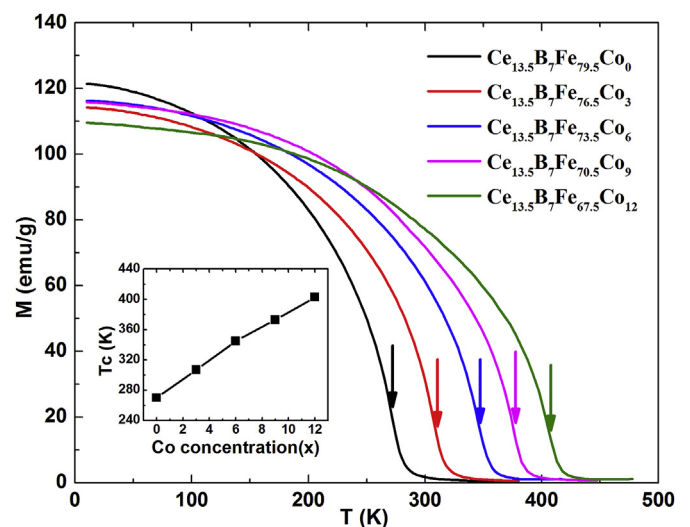


Fig. 2. Magnetization variations with temperature for all samples of $\text{Ce}_{13.5}(\text{Fe}_{79.5-x}\text{Co}_x)\text{B}_7$ amorphous ribbons under the field of 500 Oe. The inset shows the corresponding Curie temperature as a function of Co concentration.

paramagnetic state transition, is approximately 270 K. The increase of Co content x in $\text{Ce}_{13.5}(\text{Fe}_{9.5-x}\text{Co}_x)\text{B}$ leads to a continuous increase in the transition temperatures, which is 307 K, 345 K, 373 K, 403 K, respectively. The rate of increase is similar to that reported for the $\text{Nd}_4(\text{Fe}_{1-x}\text{Co}_x)_{77.5}\text{B}_{18.5}$ amorphous systems [16]. According to the theoretical calculation by T. Kaneyoshi [17] and J.S. Kouvel [18], the increase of T_c may be related to the magnitude of the exchange interactions between the atoms. The exchange interaction for the Fe–Co atom pair is much stronger than those for the Fe–Fe and Co–Co atom pairs in amorphous alloys which enhance the Curie temperature. The amorphization in Ce–Fe–B significantly reduces the T_c , and the T_c can be adjusted by controlling the atomic ratio of Co/Fe. Therefore, the required T_c can be set within a certain range to expand the usefulness of this material.

As seen in Fig. 3(a), the saturation magnetization M_s as a function of Co concentration is obtained by fitting the experimental data of $M(H)$ against H using the law of approach to saturation [19]:

$$M(H) = M_s \left(1 - \frac{a}{H} - \frac{b}{H^2} \right), \quad (1)$$

where $M(H)$ is the magnetization measured at 5 K. The M_s values have maximum, which are similar to the results for crystalline Fe–Co alloys and other amorphous Fe–Co-based alloys [20,21]. The average magnetic moment $\bar{\mu}$ was calculated by using the value of M_s , as shown in Fig. 3(b). According to previous work [21], the Ce ion is essentially tetravalent in $\text{Ce}_2\text{Fe}_{14}\text{B}$. The magnetic moment per Ce atom is suggested to be zero and it remains so throughout the Ce–(Fe,Co)–B series. Hence, only Fe and Co carry significant magnetic moments and the average magnetic moment $\bar{\mu}_{\text{Fe+Co}}$ per Fe + Co atom can be written as

$$\bar{\mu}_{\text{Fe+Co}} = \bar{\mu}_{\text{Fe}}(79.5 - x) + \bar{\mu}_{\text{Co}}x, \quad (2)$$

where $\bar{\mu}_{\text{Fe}}$ and $\bar{\mu}_{\text{Co}}$ are the effective magnetic moments per Fe atom and per Co atom, respectively. As already reported by M.F. Collins and B.G. Shen et al. [16,22], the average moment per Fe atom varies with the increase of Co concentration while the average moment per Co atom basically maintains invariable. The value of Co magnetic moments in the magnetically ordered state is remarkably different from in the paramagnetic state because of the itinerant character of magnetism [23]. Due to hybridization of B(p) and Co(d) electrons bands as a consequence of small distances between Co and B atoms [24], $\bar{\mu}_{\text{Co}}$ is approximate to $0.45 \mu_B$ and is assumed to keep the value of $0.45 \mu_B$ over the whole concentration. The composition dependence of $\bar{\mu}_{\text{Fe}}$ can be obtained from equation (2). From Fig. 3(b), $\bar{\mu}_{\text{Fe}}$ is found to increase with increasing Co concentration from $1.85 \mu_B$ for $x = 0$ to a maximal value of $2.01 \mu_B$ for $x = 6$ and then to decrease. The decrease of $\bar{\mu}_{\text{Fe}}$ can be attributed to the decrease of the coordination of nearest-neighbor cobalt atoms. A similar varying tendency has been observed for $(\text{Fe}_{1-x}\text{Co}_x)_{77.5}\text{Nd}_4\text{B}_{18.5}$ amorphous alloys [25].

The JEOL-dedicated L-TEM is further used to characterize the microstructure and magnetic domain configuration of Ce–Fe–B alloys. L-TEM was used with almost no magnetic remnant field around the sample. The microstructure of samples is featureless and no particle boundary as illustrated in Fig. 4. Based on the Selected Area Electron Diffraction (SAED) analysis, the specimen shows a diffused halo, which is a typical characteristic of amorphous materials. It also confirms the previous results of XRD that the Ce–Fe–B amorphous alloy has a good amorphous state at room temperature. The contrast between one over-focus and one under-focus TEM in Fig. 4 shows the characteristics of the magnetic domain. The Ce–Fe–B amorphous system with low magnetic anisotropy forms a vortex magnetic domain when it reaches an equilibrium state. The yellow circles indicate the position of the vortex observed by L-TEM.

It can be seen from Fig. 5 that the tree-like domain walls and in-plane vortexes are stable in samples with different Co contents. The inset in the lower left corner is the in-plane magnetization distribution of vortex which is obtained by using commercial QPt software based on intensity transfer equation (TIE). The results of electron microscope reveal that vortex magnetic domain can form spontaneously and stably at room temperature for Ce–Fe–B amorphous materials, whether Co is substituted or not. Different concentrations of Co have a slight effect on vortex density and the conditions of vortex nucleation agree well with the preceding report [26,27]. The study of magnetic vortexes has been very active in recent years for the potential of the exploration of fundamental physics and new technologies. Since there is no external field in this system and the magnetocrystalline anisotropy is negligibly small, the vortex domain mainly caused by the competition between magnetostatic energy and exchange energy. The exchange energy is smallest for parallel alignment of neighboring spins and therefore favors a uniform magnetization distribution. However, collinear spin alignments usually lead to large demagnetizing fields that increase the magnetostatic energy and hence favor flux closure or multiple domain states to reduce them. The enclosing magnetic construct depends on the balance between the above energies, and also on its shape and magnetic anisotropy. In the curling configuration, the magnetic moment rotates gradually in-plane so as not to lose too much exchange energy and starts to stand up out of the plane near the center till it completely stands up normal to the plane at the center.

The magnetization distribution of Ce–Fe–B equilibrium state is further studied by means of micromagnetic simulation. Numerical

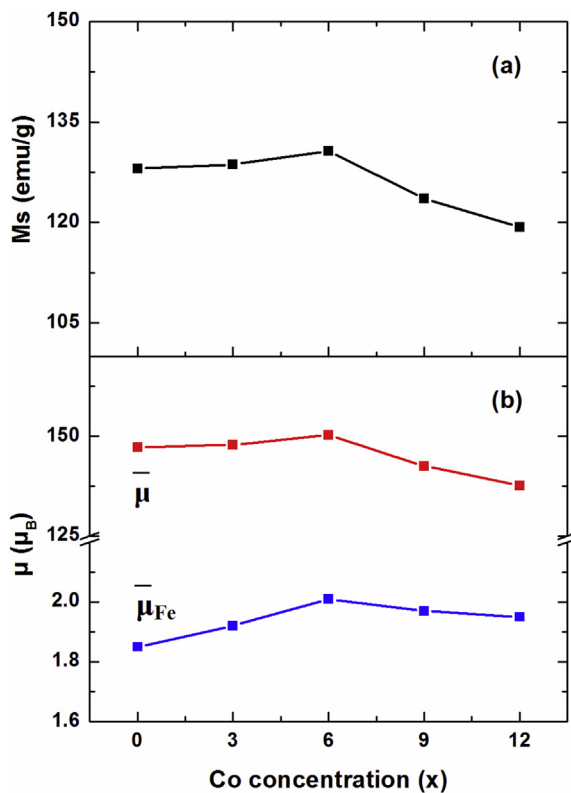


Fig. 3. The dependence of (a) saturation magnetization M_s , (b) the average moment μ and magnetic moments per Fe atom μ_{Fe} on Co concentration x for amorphous $\text{Ce}_{13.5}(\text{Fe}_{9.5-x}\text{Co}_x)\text{B}_7$ alloys.

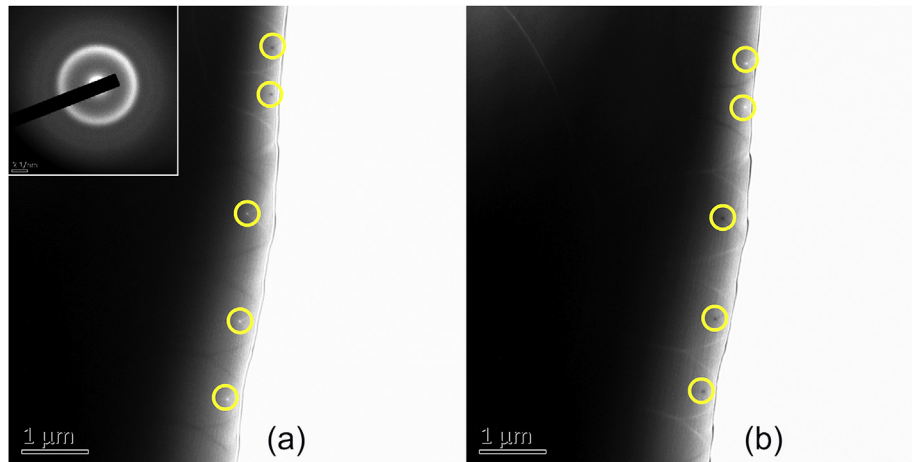


Fig. 4. The (a) overfocused and (b) underfocused image of $\text{Ce}_{13.5}(\text{Fe}_{76.5}\text{Co}_3)\text{B}_7$ amorphous alloy observed by Lorentz Transmission Electron Microscopy (L-TEM) at room temperature.

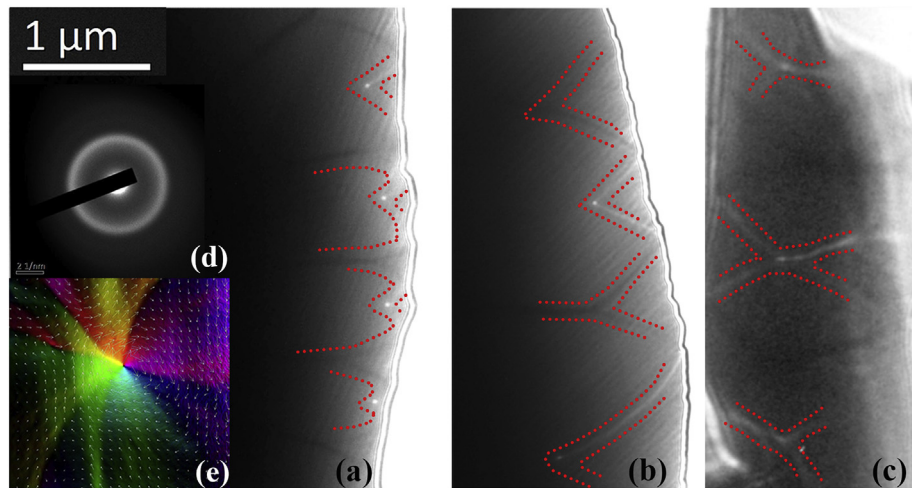


Fig. 5. L-TEM images of magnetic vortices and tree-like domain walls in (a) $\text{Ce}_{13.5}\text{Fe}_{79.5}\text{B}_7$, (b) $\text{Ce}_{13.5}\text{Fe}_{73.5}\text{Co}_6\text{B}_7$ and (c) $\text{Ce}_{13.5}\text{Fe}_{67.5}\text{Co}_{12}\text{B}_7$ amorphous samples prepared via ion milling. The inset (d) is the selected area electron diffraction with amorphous characteristic of the $\text{Ce}_{13.5}\text{Fe}_{79.5}\text{B}_7$ ribbon. (e) The in-plane magnetic texture of vortex obtained by TIE analysis with the magnitude and orientation of the magnetization depicted by the color and the arrows. (For interpretation of the references to color in this figure legend, the reader is referred to the Web version of this article.)

simulation based on the Landau–Lifshitz–Gilbert equation is performed by 3D micromagnetic package OOMMF [28]. The simulation model is set to be a magnetic strip with length $x = 500$ nm, width $y = 100$ nm and thickness $z = 10$ nm. The material parameters of Ce–Fe–B alloys are as follow: saturation magnetization $M_S = 9.3 \times 10^5$ A/m, exchange integral constant $A_{\text{ex}} = 5$ PJ/m. Starting with the magnetization in the random state (Fig. 6(a)), the system relaxes under the condition of no external field, and the corresponding ground state is solved. When the system is in a completely amorphous state, i.e., $K = 0$ J/m³, the stable and uniform magnetic vortices are formed through spontaneous relaxation. Ideal amorphous magnetic materials do not show magnetocrystalline anisotropy, but there is always a certain degree of magnetocrystalline anisotropy for practical materials. Generally, the smaller the anisotropy constant is, the better the performance of amorphous materials. However, for some special applications, such as sensor equipment, the magnetic anisotropy of materials is advantageous or even indispensable. The contribution of magnetocrystalline anisotropy to the domain structure of Ce–Fe–B equilibrium state is demonstrated by changing K value gradually. As

shown in Fig. 6(b–d), when the anisotropy strength of the system is relatively low, the ground states present vortex domains spontaneously. Meanwhile, the density and distribution of vortex domains are affected by magnetic anisotropy. Consistent with previous research results [26,29], vortex state is a typical situation of soft magnetic materials with symmetric structure when the exchange and magnetostatic interactions are mainly considered. If the K value of Ce–Fe–B increases to the permanent magnet phase, the vortex state will be destroyed by strong anisotropy and the magnetic moment is arranged in parallel along the easy axis, i.e. $+z$ direction. The magnetocrystalline anisotropy of Ce–Fe–B material will change the magnetization distribution of the equilibrium state. The findings of the magnetic vortex in series of $\text{Ce}_{13.5}(\text{Fe}_{79.5-x}\text{Co}_x)\text{B}_7$ amorphous materials will provide new insight into rare-earth resources. The preparation of thin tape or thin film samples can be used in information storage fields such as miniaturization, high magnetic recording density and high output characteristics, which can greatly expand the application of high abundance rare earth elements in functional materials.

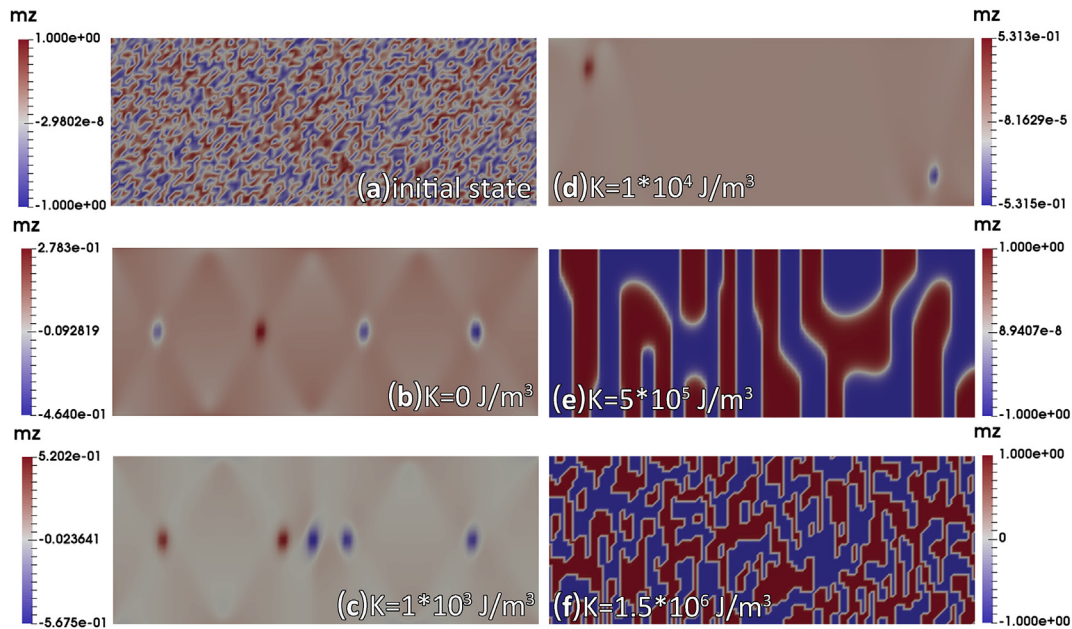


Fig. 6. (a) The initial magnetization of Ce–Fe–B alloys. (b)–(f) Schematic representation of equilibrium states in the xy plane formed at $H = 0$ Oe under different K values. m_z is the z components of magnetization and represented by regions in red (+ z) and blue (– z). (For interpretation of the references to color in this figure legend, the reader is referred to the Web version of this article.)

4. Conclusion

By using the single melt spinning method with wheel velocity of 50 m/s, the microstructure and magnetic properties of $\text{Ce}_{13.5}(\text{Fe}_{79.5-x}\text{Co}_x)\text{B}_7$ amorphous ribbons with $x = 0, 3, 6, 9,$ and 12 were investigated. The XRD analysis shows that the amorphous structure is well maintained in each sample and the ribbons are magnetically soft at room temperature as expected for amorphous materials. With increasing Co concentration, the saturation magnetization slight declines and the Curie temperature remarkably increases which enhances the maximum operating point. The L-TEM image shows the in-plane spontaneous vortex and tree-like domain walls exist spontaneously and stably in Ce–Fe–B amorphous alloys at room temperature. In addition, the magnetization distribution of equilibrium state under different amorphous degree is simulated by micromagnetism finite difference method. By changing the magnetocrystalline anisotropy, the ground states of Ce–Fe–B alloys exhibit different magnetic domain structures that can be considered for random access memory. From the perspective of balanced utilization of rare earth resources, it is of great practical significance and social value to research and develop new Ce based rare earth amorphous magnetic materials.

Author contribution statement

Dan Liu: Software, Formal analysis, Investigation, Data Curation, Writing - Original Draft, Project administration.

Tongyun Zhao: Methodology, Supervision, Funding acquisition.

Baogen Shen: Conceptualization, Methodology, Supervision, Funding acquisition.

Baohe Li: Writing - Review & Editing, Supervision, Funding acquisition.

Ming Zhang: Resources, Investigation, Writing - Review & Editing.

Shulan Zuo: Investigation, Validation.

Jun Liu: Investigation, Validation.

Sida Jiang: Investigation.

Fengxia Hu: Writing - Review & Editing.

Jirong Sun: Writing - Review & Editing.

Declaration of competing interest

The authors declare that they have no known competing financial interests or personal relationships that could have appeared to influence the work reported in this paper.

Acknowledgments

This work was supported by the National Natural Science Foundation of China (Grant Nos. 51590880), the National Key Research and Development Program of China (Grant No. 2016YFB0700903), the Inner Mongolia Science and Technology Major Project of China 2016, the Fujian Institute of Innovation, Chinese Academy of Sciences (Grant No. FJCY18040302), the Research Team Construction of Beijing Technology and Business University (Grant No. PXM2019-014213-000007), and the Research Foundation for Youth Scholars of Beijing Technology and Business University (Grant No. QNJJ2020-02).

References

- [1] B. Zhang, D.Q. Zhao, M.X. Pan, W.H. Wang, A.L. Greer, *Phys. Rev. Lett.* 94 (2005) 205502.
- [2] G. Orveillon, O.N. Senkov, J.L. Soubeyroux, B. Chevalier, S. Gorsse, *Adv. Eng. Mater.* 9 (2007) 483–486.
- [3] S. Li, R.J. Wang, M.X. Pan, D.Q. Zhao, W.H. Wang, *Scr. Mater.* 53 (2005) 1489–1492.
- [4] V. Ponnambalam, S.J. Poon, G.J. Shiflet, V.M. Keppens, R. Taylor, G. Petculescu, *Appl. Phys. Lett.* 83 (2003) 1131–1133.
- [5] Z.B. Zeng, Y.P. Shao, J.X. Du, *Electr. Eng.* 6 (2014) 116–119.
- [6] A. Inoue, B.L. Shen, C.T. Chang, *Acta Mater.* 52 (2004) 4093–4099.
- [7] A. Inoue, *Engineering* 1 (2015) 185–191.
- [8] A. Inoue, W. Zhang, T. Zhang, K. Kurosaka, *Acta Mater.* 49 (2001) 2645–2652.
- [9] B. Shen, A. Inoue, C. Chang, *Appl. Phys. Lett.* 85 (2004) 4911–4913.
- [10] R. Li, P.S.J., H. Men, T. Zhang, *Mater. Trans.* 46 (2005) 2291–2294.
- [11] B.C. Wei, T.H. Zhang, W.H. Li, D.M. Xing, L.C. Zhang, Y.R. Wang, *Mater. Trans.* 46 (2005) 2959–2962.
- [12] J. Guo, X.F. Bian, Q.G. Meng, Y. Zhao, S.H. Wang, C.D. Wang, T.B. Li, *Scr. Mater.*

- 55 (2006) 1027–1030.
- [13] Z.B. Li, L.L. Zhang, X.F. Zhang, Y.F. Li, Q. Zhao, T.Y. Zhao, B.G. Shen, *J. Phys. D Appl. Phys.* 50 (2017) 015002.
- [14] F. Yuan, Q. Li, B.L. Shen, *J. Appl. Phys.* 111 (2012) 07A937.
- [15] A. Boutahar, A. Ettayfi, G. Alouhmy, H. Lassri, E.K. Hliil, D. Fruchart, *J. Supercond. Nov. Magnetism* 27 (2014) 2401–2405.
- [16] B.G. Shen, L.Y. Yang, J.X. Zhang, F. Wo, T.S. Ning, J.G. Zhao, H.Q. Guo, W.S. Zhan, *J. Magn. Magn. Mater.* 96 (1991) 335–340.
- [17] T. Kaneyoshi, *Phys. Rev. B* 24 (1981) 2693–2700.
- [18] J.S. Kouvel, *Magnetism and Metallurgy*, Academic Press, New York, 1969.
- [19] W.F. Brown, *Phys. Rev.* 58 (1940) 736–743.
- [20] C.D. Fuerst, J.F. Herbst, E.A. Alson, *J. Magn. Magn. Mater.* 54 (1986) 567–569.
- [21] J.F. Herbst, *Rev. Mod. Phys.* 63 (1991) 819–898.
- [22] M.F. Collins, J.B. Forsyth, *Philos. Mag.* 8 (1963) 401–410.
- [23] M. Mittag, M. Rosenberg, K.H.J. Buschow, *J. Magn. Magn. Mater.* 82 (1989) 109–117.
- [24] M. Míšek, Z. Arnold, O. Isnard, H. Mayot, Y. Skorokhod, J. Kamarád, *Acta Phys. Pol.* 113 (2008) 263–266.
- [25] B.G. Shen, L.Y. Yang, J.Z. Liang, H.Q. Guo, *J. Phys.: Condens. Matter* 4 (1992) 7247–7256.
- [26] D. Liu, G. Li, X. Zhao, J.F. Xiong, R. Li, T.Y. Zhao, F.X. Hu, J.R. Sun, B.G. Shen, *AIP Adv.* 8 (2018) 056011.
- [27] S.L. Zuo, M. Zhang, R. Li, Y. Zhang, L.C. Peng, J.F. Xiong, D. Liu, T.Y. Zhao, B.G. Shen, H.F. X, J.R. Sun, *Acta Mater.* 140 (2017) 465–471.
- [28] M.J. Donahue, D.G. Porter, *OOMMF User's Guide, Versión 1.0*, National Institute of Standards and Technology, Gaithersburg, 1999.
- [29] R.P. Cowburn, D.K. Koltsov, A.O. Adeyeye, M.E. Welland, *Phys. Rev. Lett.* 83 (1999) 1042–1045.